Advanced Composites and Hybrid Materials (2023) 6:118
https://doi.org/10.1007/s42114-023-00689-2

RESEARCH

Electroconductive poly(3,4-ethylenedioxythiophene) (PEDOT) nanoparticle-loaded silk fibroin biocomposite conduits for peripheral nerve regeneration

Ane Escobar[1,2] · Aleksandra Serafin[3] · Mariana R. Carvalho[1,2] · Mario Culebras[4] · Andres Cantarero[4] · Anne Beaucamp[3] · Rui L. Reis[1,2] · J. Miguel Oliveira[1,2] · Maurice N. Collins[3,5]

Received: 11 February 2023 / Revised: 13 April 2023 / Accepted: 8 May 2023 / Published online: 30 May 2023

Abstract

Peripheral nerve injury (PNI) often clinically relies on the use of nerve grafts taken from the patient to establish a therapeutic effect, though secondary site of injury and morbidity have prompted the medical community to find alternative solutions. A new trend in the development of biomaterials arises in the form of electro-conductive biomaterials, especially for electrically active tissues such as the peripheral nerves. In this work, novel poly(3,4-ethylenedioxythiophene) PEDOT nanoparticles (PEDOT NPs) were synthetized via the mini-emulsion method and were combined with silk fibroin (SF) to create conduits for PNI repair. The synthesized PEDOT NPs-loaded SF conduits showed optimal properties for peripheral nerve substitution from the physico-chemical and biological point of view. They displayed excellent mechanical and conductivity performance with the tensile moduli reaching 6.61 ± 0.55 MPa and the conduits reaching $5.4 \cdot 10^{-4}$ S cm^{-1}, respectively. The conduits did not possess apatite-forming capacity, which were resistant to bending occlusions for angles up to 50° and to suturing. The developed conduits are promising as a novel biomaterial for applications in peripheral nerve regeneration; in vitro experiments showed that they did not allow BJ fibroblast infiltration, avoiding scar tissue formation in the lumen, and they did not show any toxic effect for Schwann cells.

Keywords Electroconductive polymers · Peripheral nerve regeneration · Nanoparticles · Nerve guidance conduits · Conductivity

Ane Escobar and Aleksandra Serafin are both first authors.

✉ J. Miguel Oliveira
miguel.oliveira@i3bs.uminho.pt

✉ Maurice N. Collins
maurice.collins@ul.ie

[1] 3B's Research Group, I3Bs—Research Institute on Biomaterials, Biodegradables and Biomimetics, University of Minho, Headquarters of the European Institute of Excellence on Tissue Engineering and Regenerative Medicine, AvePark, Parque de Ciência e Tecnologia, Zona Industrial da Gandra, Barco, 4805-017 Guimarães, Portugal

[2] ICVS/3B's—PT Government Associate Laboratory, 4710-057 Braga, Braga, Portugal

[3] School of Engineering, Bernal Institute. University of Limerick, Limerick, Ireland

[4] Institute of Material Science (ICMUV), Universitat de València, c/ Catedrático José Beltrán 2, 46980 Paterna, Valencia, Spain

[5] Health Research Institute, and AMBER University of Limerick, Limerick V94 T9PX, Ireland

1 Introduction

A peripheral nerve injury (PNI) may occur due to a traumatic event and is generally associated with injuries to limbs. Two to five percent of patients admitted to trauma centers have sustained a PNI, with resulting implications to sensory and motor function [1]. Current surgical methods for PNI treatment can be categorized as follows: direct nerve repair, nerve grafting, or artificial nerve conduit insertion.

Direct nerve repair involves the surgical stitching of the distal and proximal ends of the damaged nerve. This technique can only be applied to short lengths of damaged nerves to avoid excessive tension on the nerve, while connecting nerve ends with the required precision to allow complete motor and sensory functional repair is extremely challenging. For nerve injuries longer than 20 mm, nerve grafting is often utilized, via either an autograft or allograft [2, 3]. Despite being one of the more successful methods in terms of PNI recovery, disadvantages associated with autograft

harvesting include secondary surgery requirements, morbidity at the site of injury, loss of sensory function at the harvesting site etc. To overcome these issues, allografts are utilized, however this faces the issue of host rejection of the transplant and the subsequential need for immunosuppression [2, 3].

Such drawbacks have led the medical community and researchers to look for alternative options. Nerve conduits strive to minimize these limitations by providing guidance and support to nerve repair by means of chemotactic attraction through the proximal and distal stumps of the transected nerve [2, 3]. To further promote the growth of the axonal tracks, additional therapeutic stimulants are added to the conduits in the form of nerve growth factors or stem cells-based therapies, with Schwann cells often used as the cell of choice [4]. Key properties which must be considered are porosity, biodegradability, stiffness/flexibility, and suture ability. Tailoring these properties to achieve a favorable outcome is of paramount importance to achieve the desired tissue regenerative effect [2, 3, 5, 6].

Commercially available conduits for nerve repair include: NeuraGen, NeuroFlex, NeuroMatrix, NeuroWrap, NeuroMend, Neurotube, and Neurolac, with the majority being constructed with collagen type I, apart from Neurotube (polyglocolic acid) and Neurolac (poly(L-lactide-co-caprolactone)). Clinical use of these conduits can lead to the formation of a painful neuroma at the implementation site, especially when considering a larger diameter conduit [3, 7, 8].

Silk is produced by silkworms such as Bombyx mori or spiders. Silk Fibroin (SF) is a naturally found fibrous semi-crystalline structured protein derived from silk, with sericin being the other major silk component. SF is comprised of light and heavy chains which are connected with disulfide bonds. Glycine, alanine, and serine are the main amino acids found in the heavy chains of SF. The high glycine content influences the tight packing formation of stable β-sheet nanocrystals in the SF structure [9]. SF has been used in many TE application strategies due to its biocompatibility and tunable mechanical and degradation properties [9–11]. In particular, in vitro and in vivo studies have shown that SF can be enzymatically degraded and that it does not induce any significant inflammatory or immunogenic responses [10, 12, 13].

Recently, a novel approach of combining these conduit strategies with electroconductive components has emerged, particularly in the form of polymer composites [14]. The ideation behind this approach centers on the primary peripheral nerve function and the benefits of electrical signal transportation. By adding conductive elements into a scaffold structure and increasing its conductive properties, the cellular microenvironment can be controlled, which can lead to cellular proliferation and extension along the conduit, particularly with the addition of electrical stimulation [15–17].

A variety of electroconductive additives to create the conductive polymer composites have been used to raise the conductivity of nerve conduits including carbon based structures such as graphene oxide [18, 19], carbon nanotubes, or nano-fibers [20–23]. The safe doping levels should be carefully considered to prevent the potential toxicity of the carbon-based additives in the scaffold system [24, 25]. Conductive polymers such as aniline pentameter and polypyrrole (PPy) have also been combined with polymers such as chitosan, hyaluronic acid (HA), polycaprolactone (PCL), or silk fibroin for this purpose [26–29]. The combination of these materials must be carefully controlled not only to allow for the safe doping parameters of the conductive additive but also to consider the main component of the biomaterial. For example, the use of high molecular weight HA in PPy/HA scaffolds has been shown to not support cell adhesion of fibroblasts and neuroblastoma cells due to the highly hydrophobic nature of the scaffold [30], while the conductive polymer, poly(3,4-ethylenedioxythiophene) polystyrene sulfonate (PEDOT:PSS) has been used for many years in the electronic field, but has recently emerged as a promising material for biomedical applications [31]. However, its usage is hindered by well-known issues associated with excess PSS which negatively affects conductivity, long-term stability, specific capacity, and crucially biocompatibility [32, 33].

In this study, we present a radical new way to overcome these limitations by using a novel synthesis route for PEDOT nanoparticles (NPs) instead of the PEDOT:PSS polymer. PEDOT NPs offer many other advantages over traditional PEDOT:PSS such as tailored surface functionalization, increased electrical conductivity of scaffolds and also the ability to be dispersed in water based systems such as hydrogels, and this offers enormous potential for wide ranging tissue repair strategies. This novel hybrid PEDOT-NPs/SF composite system presents unique structure–property-performance relationships with respect to the interaction between the filler PEDOT-NPs and the SF matrix. Here, we successfully demonstrate PEDOT NPs synthesis and their successful dispersion within silk fibroin (SF) scaffolds to develop novel and improved electroconductive conduits for PNI repair.

2 Experimental

2.1 Materials and methods

2.1.1 PEDOT NPs synthesis

PEDOT NPs were synthesized by chemical oxidation polymerization via a mini-emulsion method, modified from [34],

using poly(diallyldimethylammonium chloride) (PDADMAC) as a stabilizer and Iron(III) p-toluenesulfonate hexahydrate (Fe-Tos) as oxidizer. All materials were purchased from Sigma-Aldrich (Ireland). Briefly, 1 g PDADMAC (20 wt%. H_2O_2, Sigma-Aldrich Ireland) was added to 40 mL deionized water, with ethylenedioxythiophene (EDOT) (Sigma-Aldrich Ireland) subsequently added to create a 0.037 M solution. The solution was stirred at 800 rpm for 5 min, followed by tip ultrasonication over an ice bath for 10 min. The mini-emulsion was then transferred to a round bottom flask and 10 mL of Fe-Tos 0.056 M was added dropwise. 0.001 M H_2O_2 was then subsequently added, and the solution was stirred over an oil bath at 45 °C overnight. The PEDOT NPs solution was centrifuged three times at 8700 rpm for 20 min to purify the solution and remove the supernatant. The PEDOT NPs solution was then finally resuspended in 40 mL of deionized water.

2.1.2 Silk fibroin purification

Purified SF was prepared as previously described by Yan et al. [35]. Briefly, SF was first separated from sericin, the other main protein in the silk cocoons. The cocoons were immersed in 0.02 M boiling sodium carbonate solution for 1 h, followed by rinsing with abundant distilled water. The obtained SF was then immersed in a 9.3 M lithium bromide solution at 70 °C until complete dissolution and dialyzed (benzoylated dialysis tubing, MWCO: 2 KDa, Sigma-Aldrich) for 48 h to remove impurities. The purified SF was concentrated in 20 wt% poly(ethylene glycol) solution for at least 6 h. The final concentration was determined by weighting the dry product and the SF solution was stored at 4 °C for a maximum of 5 days.

2.1.3 PEDOT NPs-loaded silk fibroin conduit synthesis

SF solution was diluted to 16 wt% with distilled water, after which it was mixed with PEDOT NPs (1.5 $mg{\cdot}mL^{-1}$), horseradish peroxidase solution (HRP type VI, 0.84 $mg{\cdot}mL^{-1}$, 100 µL), and hydrogen peroxide solution (H_2O_2, 0.36 wt%, 65 µL; Panreac, Barcelona, Spain). HRP and H_2O_2 covalently crosslink SF using enzymes [35]. Conduits without PEDOT NPs (SF Control) and with 40 µL (1% PEDOT NPs), 200 µL (5% PEDOT NPs), and 400 µL (10% PEDOT NPs) of the PEDOT NPs solution were prepared, as shown in Table 1. The previous mixture was injected within the space between two concentric cylindric molds, where the outer cylinder has a diameter of 4 mm and was made of polypropylene. Inner cylinders of 2 mm in diameter, made of iron oxide were purchased from the Neves & Neves Metalomecânica, Lda. (São Mamede do Coronado, Portugal). The system was incubated at 37 °C in order to induce gelation for a period of 30 min. After gelation, a quick immersion in liquid N_2 to remove the outer mold, followed by an immersion in ethanol to induce permanent β-sheet conformation and to remove the inner mold. Conduits were then freeze-dried after freezing at − 80 °C. The scaffold preparation schematic is shown in Fig. 1(a). Another type of conduit was also prepared; SF conduits were immersed for 4 h in 1.5 $mg{\cdot}mL^{-1}$ PEDOT NPs solution under orbital shaking, this conduit was named "soaked conduit".

Table 1 Composition of the prepared SF/PEDOT NP conduits

Sample name	PEDOT NP concentration (mg/ml)	PEDOT NP (µL)	Silk fibroin (wt%)
SF control	1.5	0	16
PEDOT 1%	1.5	40	16
PEDOT 5%	1.5	200	16
PEDOT 10%	1.5	400	16
Soaked conduit	1.5	-	16

2.1.4 Scanning electron microscopy (SEM)

PEDOT NPs were visualized via SEM analysis with Hitachi SU70 SEM at an imaging voltage of 10 kV. A drop of NPs solution was left to dry onto a glass slide to obtain a NP film. PEDOT NPs were coated with gold sputtering before the SEM analysis.

The morphology and microstructure of the conduits were evaluated by SEM (JSM-6010 LV, JEOL, Japan). Conduits were previously coated with gold sputtering at 6 mA, using a Hitachi coater.

2.1.5 Dynamic light scattering

ζ-potential and particle size of the PEDOT NPs were measured using a particle size analyzer (Zetasizer Nano ZS, Malvern Instruments, Malvern, UK). NPs were diluted to low concentration in a 0.3 M KCl aqueous solution.

2.1.6 Stereomicroscopic evaluation

For macroscopic evaluation the hydrated conduits were cut in half and viewed under a Stereo Microscope (Schott KL 200, model Stemi 1000, Zeiss, Germany).

2.1.7 Fourier-transform infrared spectroscopy (FTIR)

The chemical composition and conformation of the conduits was analyzed with an IRPrestige-21 (Shimadzu, Japan) by attenuated total reflectance (ATR) FTIR spectroscopy. The spectra were obtained from an average of 32 scans between 3500 and 500 cm^{-1} taken at 4 cm^{-1} resolution.

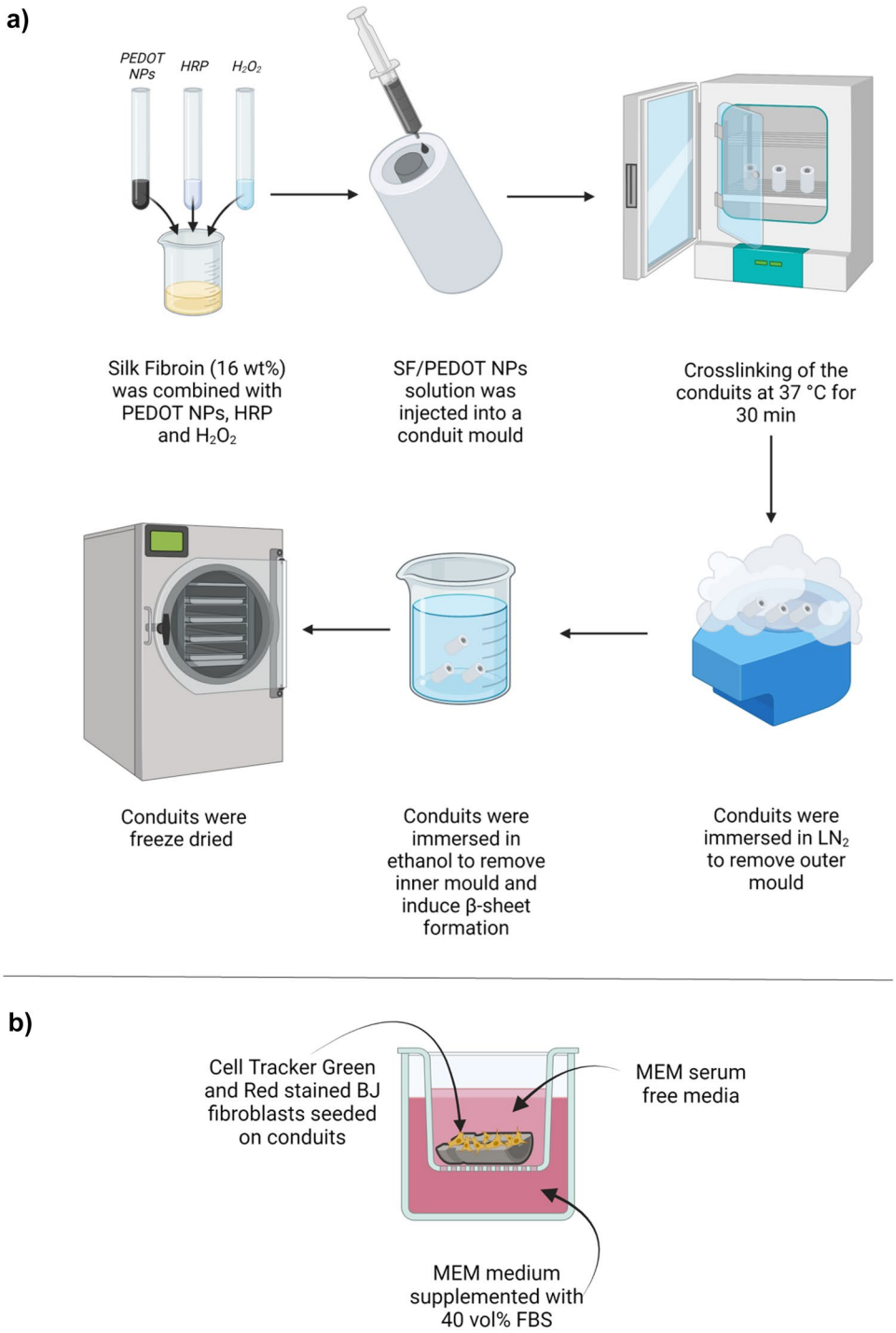

Fig. 1 **a** Schematic of the synthesis of the SF/PEDOT NP conduits. **b** Schematic of in vitro BJ fibroblast cellular permeability assay using a modified Boyden chamber (images created with BioRender.com)

2.1.8 X-ray photoelectron spectroscopy (XPS)

X-ray photoelectron Kratos Axis-Supra instrument equipped with aluminum Kα monochromatized radiation X-ray source, within the ESCApe software was used to perform the photoelectron analysis of the film samples. The binding energies (BEs) positions were referenced to the C1s on non-sputtered surfaces. Charge referencing was done by setting the binding energy of C1s photo peak at 285.0 eV C1s hydrocarbon peak. Furthermore, an electron flood gun was employed to minimize surface charging (charge compensation). The measurement was done in a Constant Analyser Energy mode (CAE) with a 160 eV pass energy for survey spectra and 20 eV pass energy for high-resolution spectra of carbon (C1s), oxygen (O1s), sulfur (S2p), and nitrogen (N1s). The atomic concentrations were determined from the

XPS peak areas using the Shirley background subtraction technique and the Scofield sensitivity factors.

2.1.9 Differential scanning calorimetry (DSC)

DSC was performed in a DSC Q100 Model of T. A. Instruments to study the thermal stability and changes in crystallinity over a range of temperatures. The conduits were crushed to obtain a powder, and a known mass was placed in an aluminum pan and a lid was crimped onto the pan. The pan was then placed in the sample cell of a DSC module. Under N_2 gas purge (50 mL·min^{-1}), temperature was first equilibrated to – 35 °C and increased at a rate of 10 °C·min^{-1} until the material degrades. The temperatures were obtained for each peak in the resulting curve.

2.1.10 Mechanical testing

An Instron universal mechanical testing machine (Model 5540, USA) was used to study the mechanical properties of the conduits following the ASTMC749-08 standard method with a load cell of 50 N. Samples were fixed using a grip and were stressed with a cross-head speed of 2 mm·min^{-1} until rupture. Strain–stress curves were obtained for 5 hydrated samples in phosphate buffered saline (PBS) 10 mM at 37 °C overnight, with a 3 mm length to determine the Young's modulus by the tangent method.

Kinking tests were performed with 3 cm length conduits by bending them up to 50° in a metallic flexible 0.5 mm wire and macroscopically assessing the bending point.

The suturability was assessed by means of inserting a 4–0 surgical suture at the place where peripheral nerve suturing would be performed, which was 2 mm from the end of the conduit considering its long axis and strain to the rupture point.

2.1.11 Electrical conductivity

The electrical volume conductivity measurements were carried out on the conduits using a KEITHLEY 2460 and KEITHLEY SMU 2635B source meter, respectively. Electrodes were placed at a 14 mm distance and resistivity was measured when a voltage of + 10 V was applied, at atmospheric pressure and in controlled humidity conditions. Three replicates of each studied conduits were measured.

2.1.12 Bioactivity test in SBF

An acellular simulated body fluid (SBF) was prepared as described by Kokubo et al. for the in vitro bioactivity tests [36]. The SBF contains the same ions as human blood plasma, at nearly equal concentrations. Conduits were immersed in freshly prepared SBF for 1, 15, and 30 days at 37 °C; they were then rinsed with distilled water and left to dry. The presence or absence of a calcium-phosphate layer on their surface was determined using a SEM equipped with an energy dispersive spectroscope (EDS) (INCAx-Act, PentaFET Precision, Oxford Instruments), at an accelerated voltage of 15 kV.

2.2 Cell culture of mesenchymal stem cells, immortalized human Schwann cells, and immortalized human skin BJ fibroblasts

Mesenchymal stem cells (MSCs) were grown in Modified Eagle's Medium alpha (Sigma-Aldrich) supplemented with 20% fetal bovine serum (FBS), 1% GlutaMAX, and 1% penicillin/streptomycin. Immortalized Schwann cells (SCs, sNF96.2, ATCC) were cultured in High Glucose Dulbecco's Modified Eagle's Medium (Sigma-Aldrich) supplemented with 10% FBS, 1% penicillin/streptomycin, and 1% sodium pyruvate, in noncoated cell culture flasks. BJ fibroblasts (BJ, CRL-2522, ATCC) were cultured in Eagle's Minimum Essential Medium (Sigma-Aldrich), supplemented with 10% FBS and 1% penicillin/streptomycin and 1% sodium pyruvate. Cell medium was changed every 2–3 days and the cells were kept at 37 °C and 5% CO_2.

2.2.1 Biocompatibility of PEDOT NPs

PEDOT NPs cytotoxicity was evaluated with MSCs seeded into a 96 well-plate at a density of $0.025 \cdot 10^6$ cells well^{-1}. MSCs were cultured in presence of 1%, 5%, and 10% of PEDOT NPs for 96 h and medium with 10% Alamar Blue (AB) added and incubated for 5 h for cell viability analysis. AB dye yields a fluorescent signal when incubated with metabolically active cells. The fluorescent emission was measured with Cytation5 (BioTek, USA) at excitation/emission wavelengths of 540/590 nm. Cells incubated in medium only were used as control.

2.2.2 Biocompatibility of PEDOT NPs-loaded silk fibroin conduits

The viability of Schwann cells and BJ fibroblasts was followed with AB. Sterilized conduits were cut at 14 mm and in halves for direct cell seeding on top of the inner concave surface. Conduits were placed in non-adherent culture plates, while adherent culture plates were used as both cell type growth control. A 20 µL drop at 10^5 cells mL^{-1} was placed on the conduits and cells were left to adhere for 1 h. Then, 500 µL of medium was added to each well. As controls, 500 µL of cells at a concentration of 10^4 cells mL^{-1} were seeded. After 1, 3, and 7 days in culture, specific cell culture medium containing 20% AB was added to the different culture wells. The system was incubated for 3.5 h, and

fluorescence was monitored at 590 nm emission wavelength (excitation wavelength 530 nm), using a FL 600, Bio-Tek Instruments microplate reader. PBS was used to remove the excess of AB reagent and fresh culture medium was added in its place after each AB determination. Corrections to control group of cell density and available area for them to grow were made.

The qualitative evaluation of viability of Schwann Cells within PEDOT NPs-loaded SF conduits was followed with a LIVE/DEAD assay at 24 and 72 h. Briefly, cell-laden conduits were washed three times with PBS and incubated for 30 min, at 37 °C in dark with 10^{-6} M Calcein AM and $1.5 \cdot 10^{-6}$ M propidium iodide. Samples were then washed with PBS three times and imaged using a transmitted and reflected light microscope (Axio Imager Z1m, Zeiss, Jena, Germany).

2.2.3 In vitro cellular permeability assay (using a modified Boyden chamber)

Cell migration assay was designed to verify the cellular permeability of the PEDOT NPs-loaded SF conduits to BJ fibroblasts, using HTS Corning FluoroBlokTM Cell Culture Inserts (24 well) with an 8 µm pore size (Becton Dickinson, USA). For direct cellular seeding, conduits with 4 mm in length were cut longitudinally (to fit the insert) and in halves. Conduits were first hydrated for 1 h in sterile PBS. BJ fibroblasts were prelabelled with $5 \cdot 10^{-3}$ M Cell Tracker Red (Invitrogen, CA, USA) for imaging, and $5 \cdot 10^{-3}$ M Cell Tracker Green (Invitrogen, CA, USA) for plate reader measurements for 30 min, and then seeded directly in the internal and concave surface of the conduit at a cell density of $8 \cdot 10^3$ cells per conduit. Cell Tracker probes freely pass-through cell membranes and once inside the cell they were transformed into cell-impermeable reaction products well retained in living cells through several generations, but not transferred to adjacent cells in a population. Cellular adhesion was allowed to occur in a normal nonadherent 24 well plate for 3 h, using a serum free medium. Cell-laden constructs were then moved to the upper chamber of the HTS Corning FluoroBlokTM Cell Culture Inserts, making sure the external and convex surface of the conduit was in contact with the insert surface. In the upper chamber, where the construct was placed, MEM serum-free medium was added and in the lower chamber, MEM medium supplemented with 40 vol% FBS was added, in order to serve as a chemoattractant gradient, as shown in Fig. 1(b). As a positive control, the same cellular density was directly seeded in the upper chamber. At different time points (24, 48, and 72 h), fluorescence intensity from the bottom (basal side) was measured using a microplate spectrofluorometer (FL 600, Bio-Tek Instruments) in a scan bottom-reading mode, at excitation/emission wavelengths of 485/520 nm. Fluorescence images of cells that migrated through the conduit wall after 48 h were collected using an inverted fluorescence microscope (model TCS SP8, Leica, Germany).

2.2.4 Statistical analysis

The statistical ANOVA analysis were performed in the OriginPro 2016 software. Fisher's tests were performed to determine statistically significant differences with a $p < 0.05$.

3 Results and discussion

3.1 PEDOT NPs characterization

The synthesized PEDOT NPs form a blue/black solution when re-suspended in DI water. Visualization of the NPs conducted by means of SEM imaging shows a high concentration of stable NP with a round morphology, as can be seen in Fig. 2(a). ImageJ image analysis indicates that the PEDOT NPs have an average diameter of 187.3 ± 20.2 nm, as shown in Fig. 2(b). The NPs ζ-potential measured by DLS showed to be $+19.2 \pm 0.5$ mV indicating NPs were stable in aqueous solution, as shown Fig. 2(c).

3.2 Macro and microstructure of the PEDPT NPs-loaded SF conduits

When SF conduits were combined with PEDOT NP solutions, the presence of PEDOT NPs was easily observed in Fig. 3(a), with conduits display an increasing darker grey colour as a function of PEDOT NPs concentration. Stereomicroscopic images of hydrated conduits, Fig. 3(b), reveal their macroscopic structure. For conduits prepared with PEDOT NPs at differing concentrations (1%, 5%, and 10%, Fig. 3(b) third, fourth, and fifth rows, respectively), the distribution of the polymer was homogeneous. However, when SF conduits were soaked in PEDOT NPs (Fig. 3(b) second row), it was observed that PEDOT were not distributed uniformly throughout the conduit, as darker patches, associated with PEDOT NPs, were observed.

SEM images of conduit cross-sections (Fig. 4, first column) show wall thickness of ~ 400 µm for all conduits with a total conduit diameter of ~ 2.5 mm, which does not vary between different conduits. Figure 4 also shows the microstructure of the conduits in the second and third columns, respectively. Cross-sections reveal a highly interconnected porous microstructure for all conduits, which is an important factor to facilitate nutrient and waste exchange [37–39]. In peripheral nerve regeneration, porosity plays an important role for micro blood vessel penetration. In longer nerve gaps element, nutrient and oxygen supply is hindered through the longitudinal axis

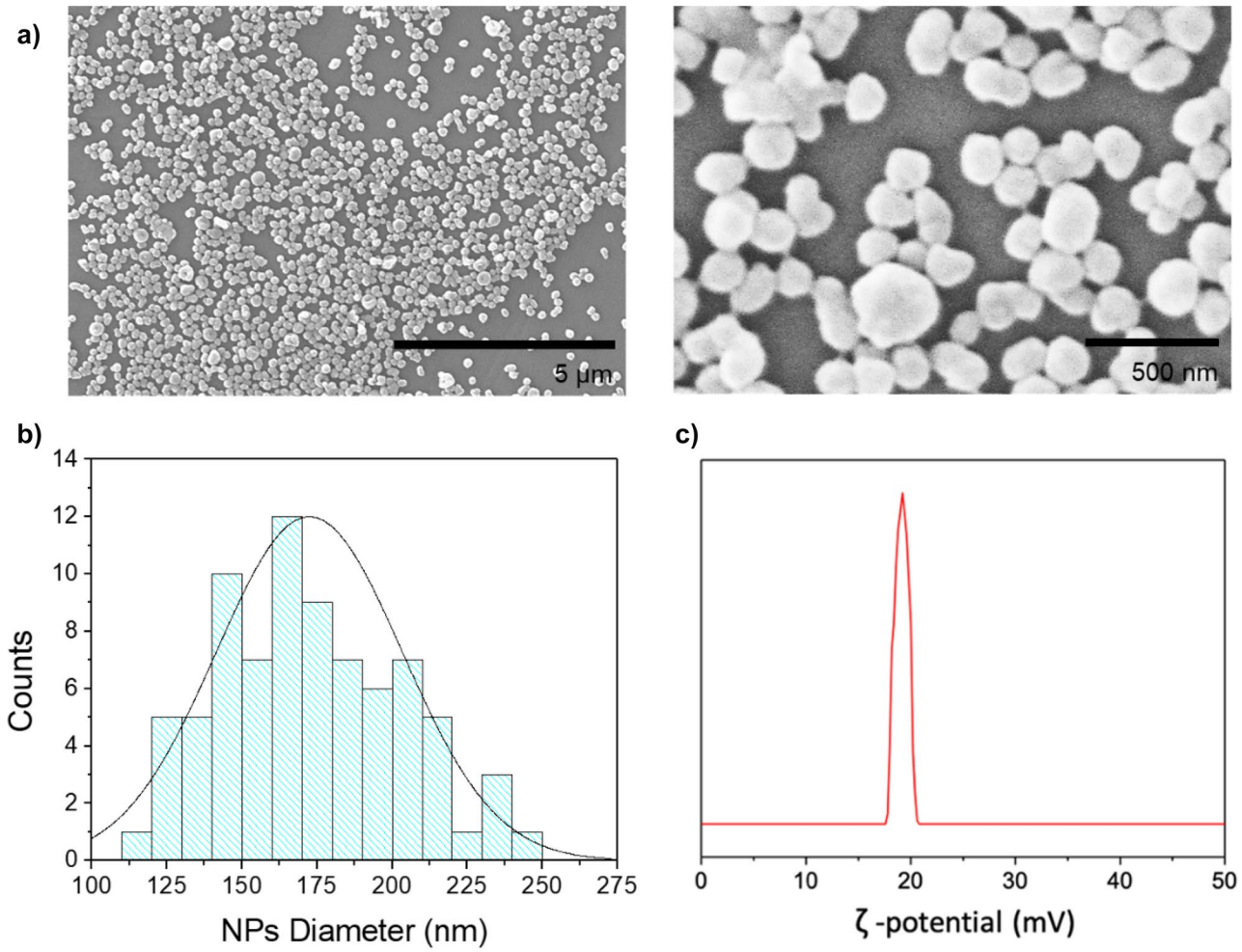

Fig. 2 PEDOT NPs characterization. **a** SEM micrographs, **b** plot of NPs diameter size distribution, and **c** plot of the measured ζ-potential

of the graft, resulting in poor cellular growth and behaviour. The conduits reported here possess a pore diameter of 2.79 ± 0.2 µm for the PEDOT NP conduits with barely any variation between the PEDOT NP concentrations, while the SF conduit has an average pore diameter of 2.6 ± 0.37 µm. Conversely, the PEDOT NP soaked conduit has the highest value for the cross-sectional porosity diameter at 4.2 ± 0.15 µm. This variation is potentially due to the inner soaking of the conduits in PEDOT NP/water solution before the freezing process. This forms larger ice crystals within the architecture and when the conduits were lyophilised, these ice crystals were removed, leaving behind larger pores in the geometry. If pore size in the conduit is too large (above 10 µm), non-neural cells can enter into the lumen and form scar tissue, thus leading to impaired nerve regeneration [40, 41]. Fibroblasts measure around 8 µm in diameter [42]. Therefore, pore size needs to be optimal to achieve a balance between the outward diffusion of growth factors and scar tissue formation reduction. In this case, the pore size below 10 µm was optimal for the desired purpose of PNI regeneration [40].

3.3 Chemical composition of the conduits

β-sheet conformation was related to semi-crystalline state and low water solubility. The conformation of the developed conduits was evaluated by ATR-FTIR to confirm the transition from amorphous to crystalline state and the results are shown in Fig. 5(a). The intermediate structure in the form of the hydrogel was characterized by an amorphous state; however, all final conduits displayed absorbance peaks at 1627 and 1520 cm^{-1}, which are characteristic of β-sheet conformation (amide I and II band) [43]. Moreover, at 1262 cm^{-1} a shoulder appears, which corresponds to the amide III band [44]. The major silk fibroin band was centered at 3300 cm^{-1}, which corresponds to the stretching vibration of the NH moiety of the amide group involved in both inter- and intramolecular hydrogen bonds [45]. FTIR

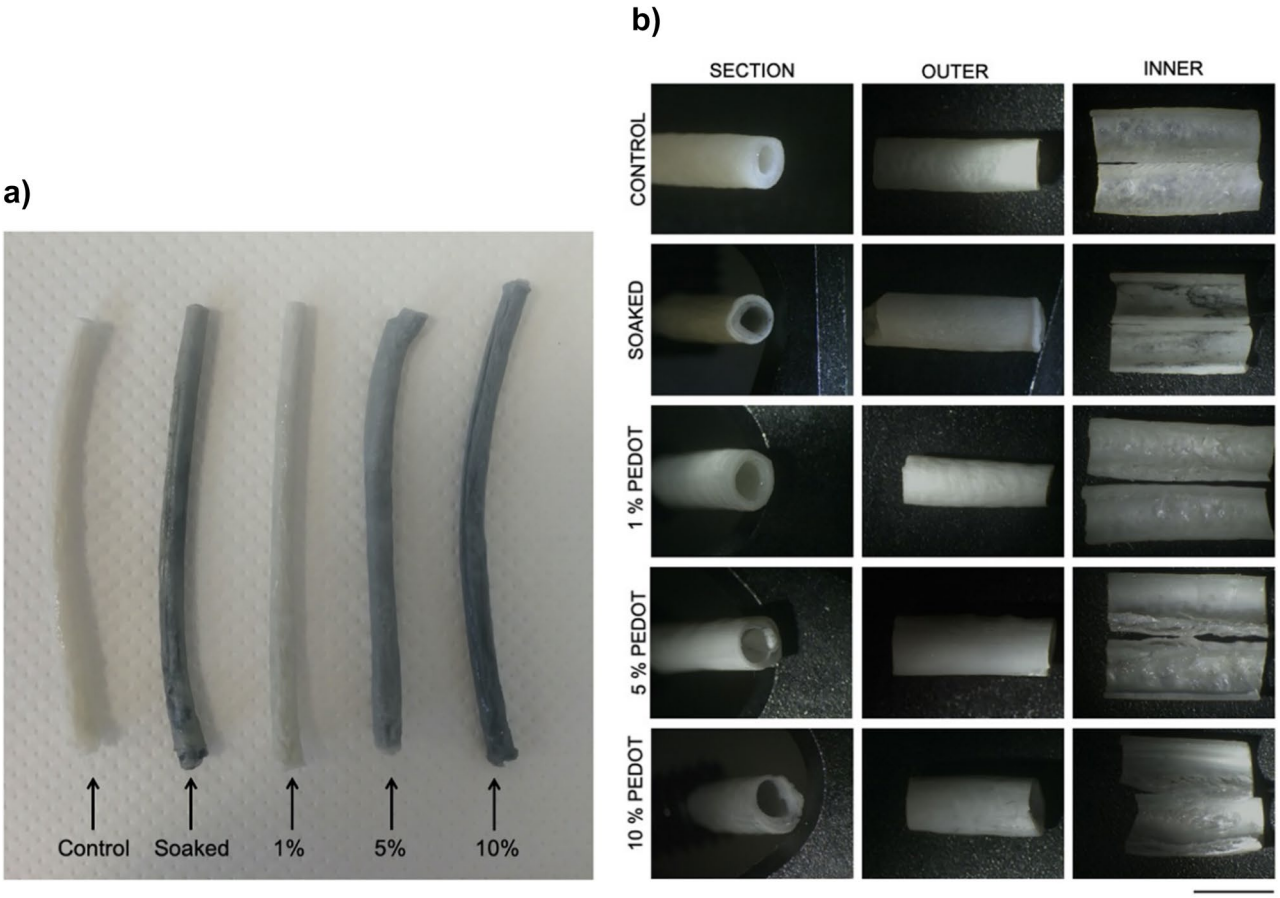

Fig. 3 Hydrated conduits. **a** Photos of the conduits; from left to right: control SF conduit, SF conduit soaked in PEDOT NPs and 1, 5, and 10% PEDOT NPs-loaded SF conduits. **b** Stereomicroscope representative images of the section (first column), outer wall (second column), and inner wall (third column) of control SF conduit (first row), SF conduit soaked in PEDOT NPs (second row), and 1% (third row), 5% (fourth row), and 10% (fifth row) PEDOT NPs-loaded SF conduits. Scale bar = 1 cm

spectra of PEDOT NPs shows its typical bands at 1515, 1315, 1187, 1138, 1083, 1048, 972, 915, 832, and 674 cm^{-1} [46]. The bands at approximately 1515 and 1315 cm^{-1} were assigned to asymmetric stretching mode of C = C and inter-ring stretching mode of C-C, respectively. The bands appearing at around 1187, 1138, 1083, and 1048 cm^{-1} were attributed to the C-O-C bending vibration in ethylenedioxy group, while the bands at 972, 915, 832, and 674 cm^{-1} were the characteristic bands of stretching vibrations of the C-S-C bond in thiophene ring [47–49].

Figure 5(b) shows DSC spectra of PEDOT NPs, and the different SF conduit formulations with the conductive NPs. The first broad peak that appears in every spectrum was associated to the evaporation of water, which was reported in the range between 10 and 110 °C. However, when the spectra of the conduits, without or with PEDOT NPs, were analyzed, it was observed that there was no exothermic crystallization peak at 229 °C, which was attributed to the transition from amorphous to crystalline structure [50]. This was due to the treatment in ethanol during the conduit synthesis, which induces permanent ß-sheet in the SF [51]. The peak at around 280 °C was associated with the melting point of the conduits [50].

XPS surface measurements were used to examine the chemical composition of the surface of the conduits. The survey analysis (Fig. 6 left) displays the presence of O, N, and C; however, with zoom (Fig. 6 right) S2p bands were observed in the PEDOT sample and in the SF conduits that were soaked in PEDOT NPs. These bands present a doublet at binding energies between 168 to 170 eV for oxidized S in $R\text{-}SO_3^-$ for the sulfonate ions in the dopant part of PEDOT. Bands between 164 and 165 eV were assigned to the thiophene ring of EDOT repeat units [52]. Pure PEDOT samples do not contain any nitrogen, as this element was brought by the surfactant PDADMAC for the nanoparticles synthesis [53]. Table 2 displays the elemental composition of the silk fibroin conduits, relative to carbon. Nitrogen was only present in the PEDOT NP and its relative amount increases regularly as the PEDOT NP concentration increases which was due to the presence of the PDADMAC surfactant [53].

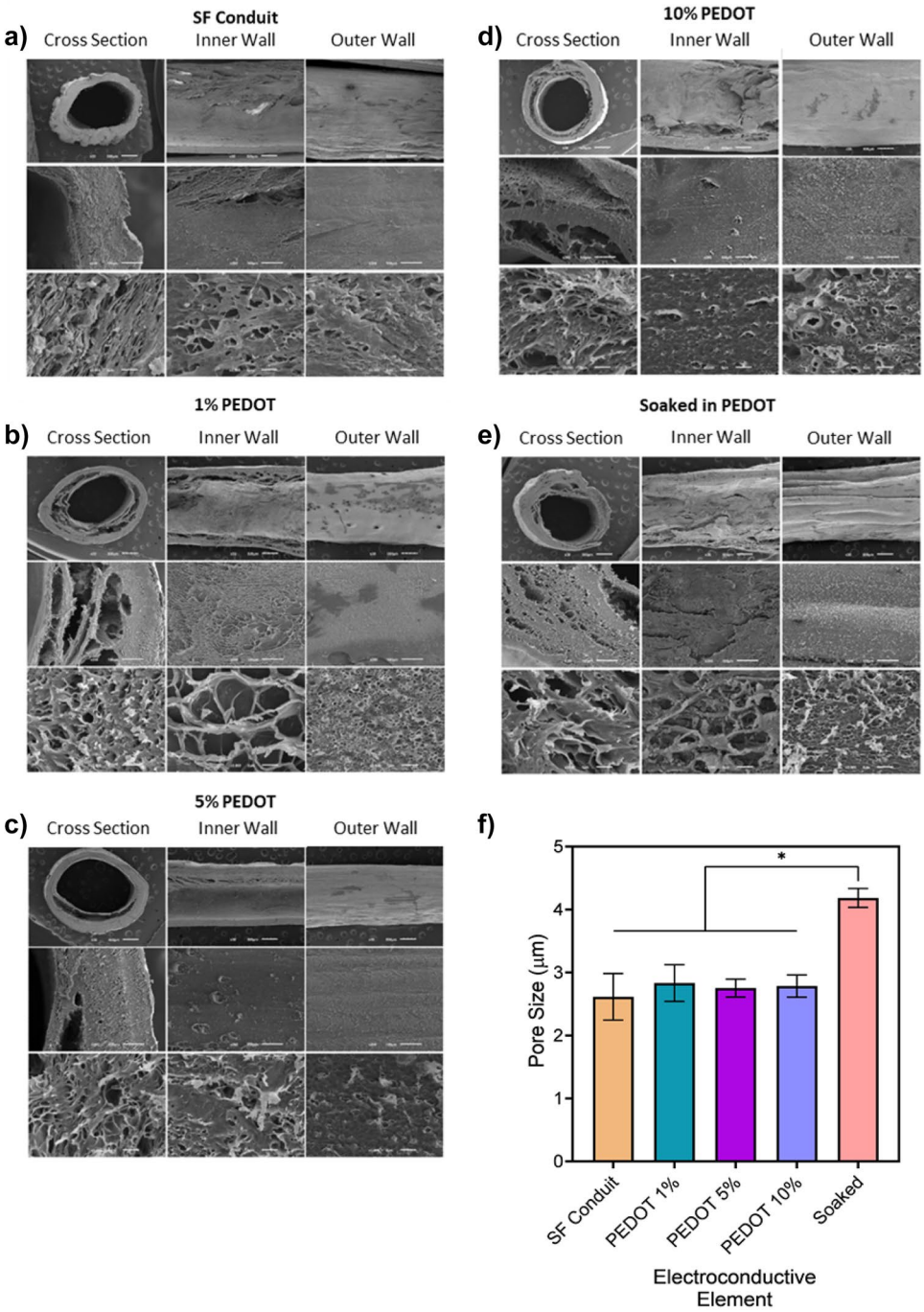

Fig. 4 SEM microphotographs of the SF conduit **a**, 1% **b**, 5% **c**, and 10% PEDOT NPs-loaded SF **d** conduits and PEDOT NPs-soaked conduit **e** and cross-section (first column), inner wall (second column), and outer wall (third column), taken at a magnification of × 30 (first row, scale bar = 500 µm), × 200 (second row, scale bar = 100 µm) and × 3,000 (third row, scale bar = 5 µm). **f** Pore diameter quantification of scaffold cross-section, (*$p < 0.05$, ($n = 5$, mean ± SD))

The deconvoluted C1s spectra for the silk fibroin conduits is presented in Fig. 7 and the carbon functionalisation in Table 2. Pure PEDOT presents typical binding energy levels with C = C, C–S, and C = C-O bonds at 284.8 eV, 285.7 eV, and 286.6 eV respectively. The PEDOT XPS spectrum also presents satellite π to π^* peak which was consistent to conjugated systems [52]. The peak at 284.8 eV corresponds to carbon–carbon bonds, both single and double. The control sample presents the highest amount of carbon - carbon bonds with 62% of overall intensity on that oxidation level. As the amount of PEDOT NP loading increases at the surface of the sample the amount of C-C bonds decreases while that of C–S (binding energy of 285.7 eV) increases. Interestingly, the composition levels for the soaked conduits and the 1% PEDOT conduct were similar at surface levels (XPS) while they were closer to that of the 5% PEDOT EDS levels (see Table 3). This can be interpretated as a higher penetration rate of the PEDOT NP during soaking, causing the PEDOT NP to get deeper into the conduits due to the increased pore size observed in SEM images. The presence

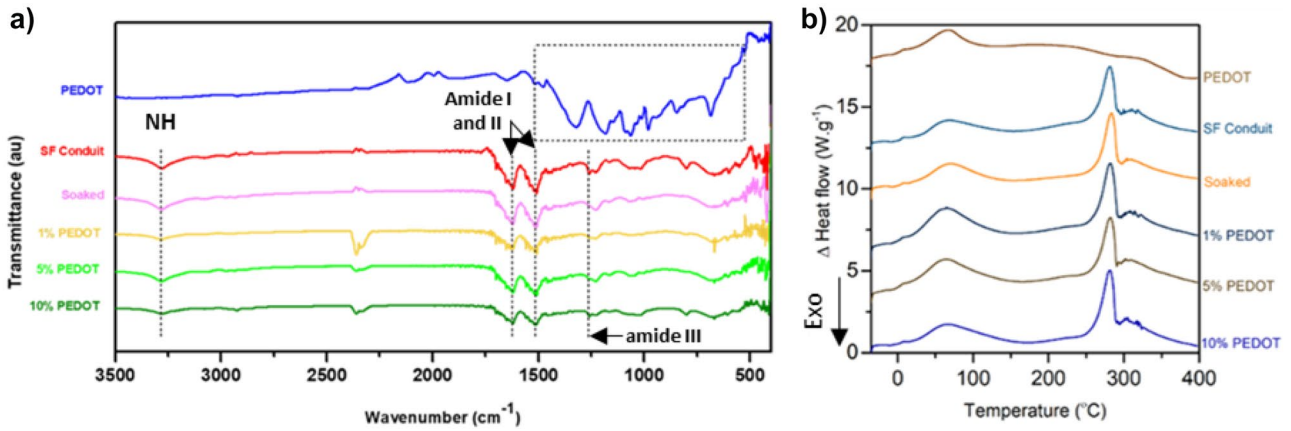

Fig. 5 Conduits chemical characterization: **a** FTIR spectra of the different silk fibroin conduits. Similar spectra are obtained regardless of the thickness of the amount of PEDOT NPs present in the conduit. The spectra for SF conduits (without and with PEDOT NPs) show characteristic peaks at 1627 cm^{-1} (amide I), 1520 cm^{-1} (amide II), and 1262 cm^{-1} (amide III) and 3300 cm^{-1} (N–H stretching vibration). The PEDOT NPs spectra shows its typical bands at 1515 cm^{-1} (C=C asymmetric stretching), 1315 cm^{-1} (C-C inter-ring stretching), 1187, 1138, 1083, and 1048 cm^{-1} (C-O-C bending vibration) and 972, 915, 832, and 674 cm^{-1} (C-S-C bond stretching vibrations). **b** DSC spectra (Exo down) of PEDOT NPs, SF conduit, SF conduit soaked in PEDOT and 1, 5, and 10% of PEDOT NPs-loaded SF conduits

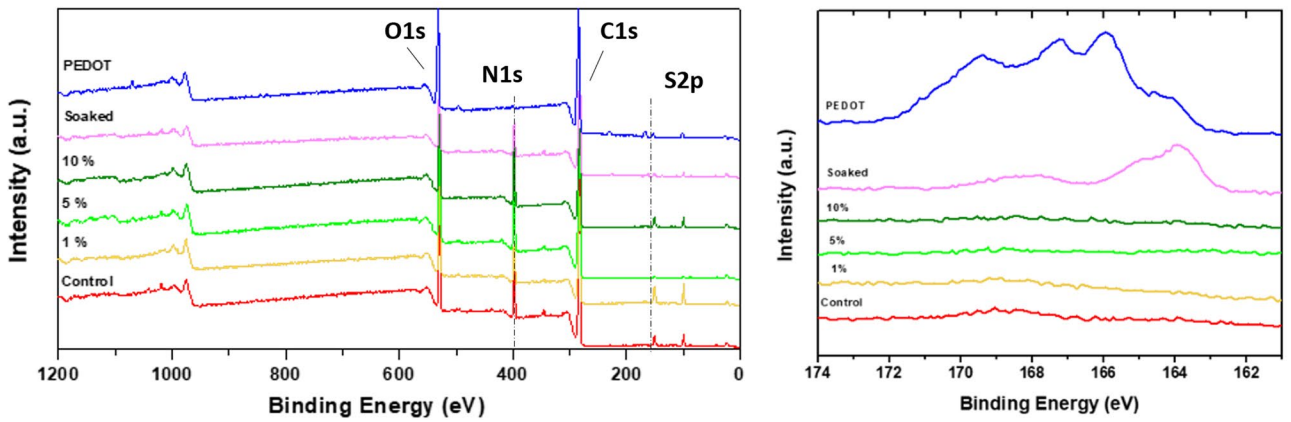

Fig. 6 XPS spectra of control SF conduits, PEDOT, SF conduits soaked in PEDOT NPs and with 1, 5, and 10% PEDOT NPs-loaded SF conduits. Left: general overview of the spectra and right: zoom in of the spectra to see the S2p peaks

Table 2 Relative mass concentration of O and N against C of control SF conduits, conduits with 1, 5, and 10% PEDOT NPs, SF conduits soaked in PEDOT NPs and PEDOT NPs obtained from the XPS spectra measurements

	Relative elemental mass concentration vs C1s		C1s atomic bonds		
	O1s/C1s	N 1 s/C1s	C=C-O	C-S	-C-C/C=C
Binding energy (eV)	531.7	400.0	286.6	285.7	285.1
SF conduits	31.39 ± 0.29	14.92 ± 0.26	17.6 ± 0.3	4.1 ± 0.22	62.0 ± 0.5
1% PEDOT	30.43 ± 0.39	14.84 ± 0.37	22.35 ± 0.3	6.5 ± 0.2	47.4 ± 0.4
5% PEDOT	42.57 ± 0.41	16.78 ± 0.34	21.9 ± 0.6	7.5 ± 0.4	47.6 ± 0.6
10% PEDOT	33.71 ± 0.29	23.75 ± 0.29	16.2 ± 3.2	20.9 ± 4.3	37.6 ± 3.2
Soaked sample	42.45 ± 0.41	26.57 ± 0.37	18.6 ± 2.3	9.0 ± 1.7	54.0 ± 2.2
PEDOT powder	36.75 ± 0.38	-	12.2 ± 0.3	22.2 ± 0.3	50.0 ± 0.4

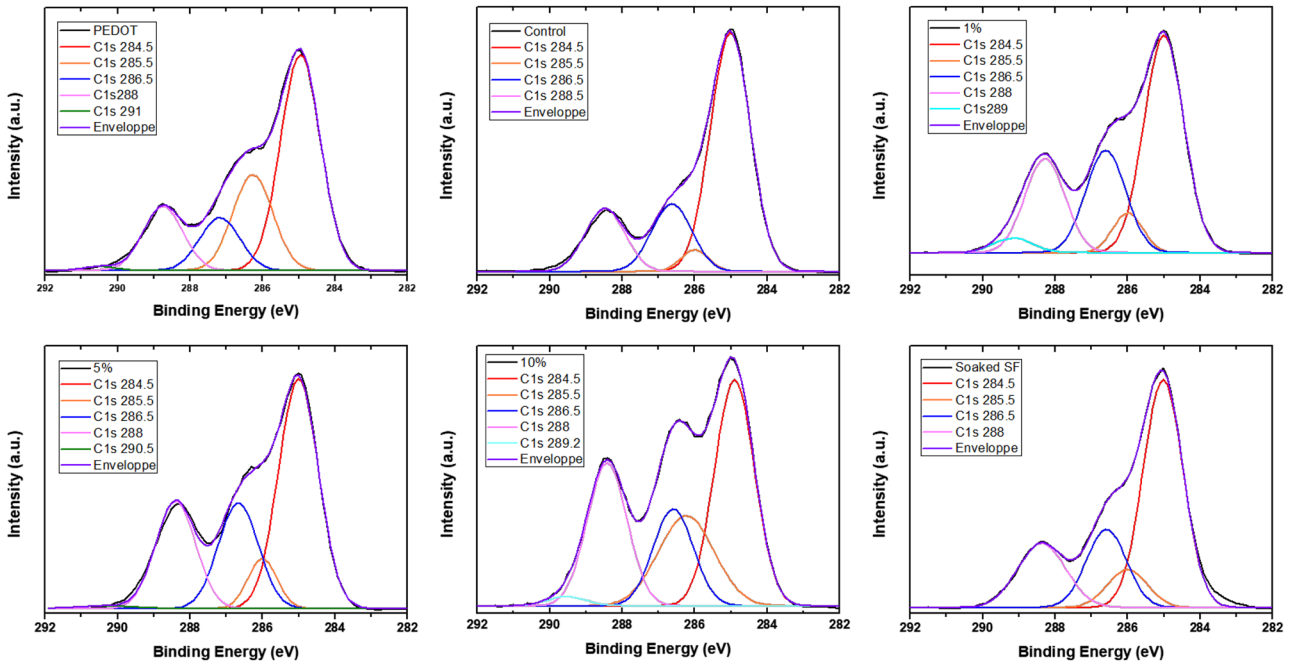

Fig. 7 Fits of the C1s XPS spectra for control SF conduits, PEDOT, SF conduits soaked in PEDOT NPs and with 1, 5, and 10% PEDOT NPs-loaded SF conduits

of sulfur in the silk fibroins loaded with PEDOT NPs was below the limit of resolution of the EDX.

3.4 Mechanical properties of the conduits

The effect of the PEDOT NP loading on the mechanical properties of the conduits was investigated by tensile testing, with the results presented in Fig. 8. Mechanical properties have been demonstrated to be a highly important regulator of axonal regeneration and elongation [54]. The surrounding musculoskeletal system exerts mechanical loads to the nerves to conduct action potentials [55]. Nerve guidance conduits should not outperform the mechanical properties of peripheral nerves themselves as this causes discontinuous elasticity between the conduit and the growth of the new tissue [56, 57]. In the resting position, peripheral nerves are subjected to tensile loads, experiencing ~ 12% strain [58]. Therefore, at this strain nerve conduits must be able to elongate. To test the mechanical behavior, conduits were subjected to force until rupture, as shown in Fig. S1 as representative images of SF and 1% PEDOT NPs-loaded SF conduits. Strain–stress curves representing the 5 tested conduits with a dashed line at the tensile stress at 12% of strain is highlighted (Fig. S2). From these curves, the Young's modulus was calculated though the tangent method and is shown in Fig. 8(b).

Table 3 EDS results revealing the elemental composition and their relative abundance present on the surface of control SF conduits, 1, 5, and 10% PEDOT NPs-loaded SF conduits, and SF conduits soaked in PEDOT, after a bioactivity assay for 30 days. The wt% stands for percentage by weight and σ stands for standard deviation

30 days	SF conduits		1%		5%		10%		Soaked	
	wt%	σ	wt%	σ	wt%	σ	wt%	σ	wt%	σ
C	49.4	1.7	52.9	1.5	49.4	1.4	48.6	1.6	50.7	2.0
O	26.4	1.1	25.2	0.9	26.6	0.9	26.9	1.1	27.3	1.3
N	21.3	2.4	21.4	2.0	23.0	1.9	23.0	2.2	18.0	2.8
Si	1.4	0.1	0	0	0.4	0	0.6	0.1	1.6	0.1
Na	0.5	0.1	0.2	0.1	0.2	0.1	0.4	0.1	0.4	0.1
Cl	0.8	0.1	0.2	0	0.3	0	0.3	0	0.7	0.1
Ca	0.1	0	0	0	0.1	0	0.1	0	0.3	0.1
K	0.1	0	0	0	0	0	0	0	0	0.1
P	0	0	0	0	0.1	0	0	0	0.2	0.1
S	-	-	-	-	-	-	-	-	-	-

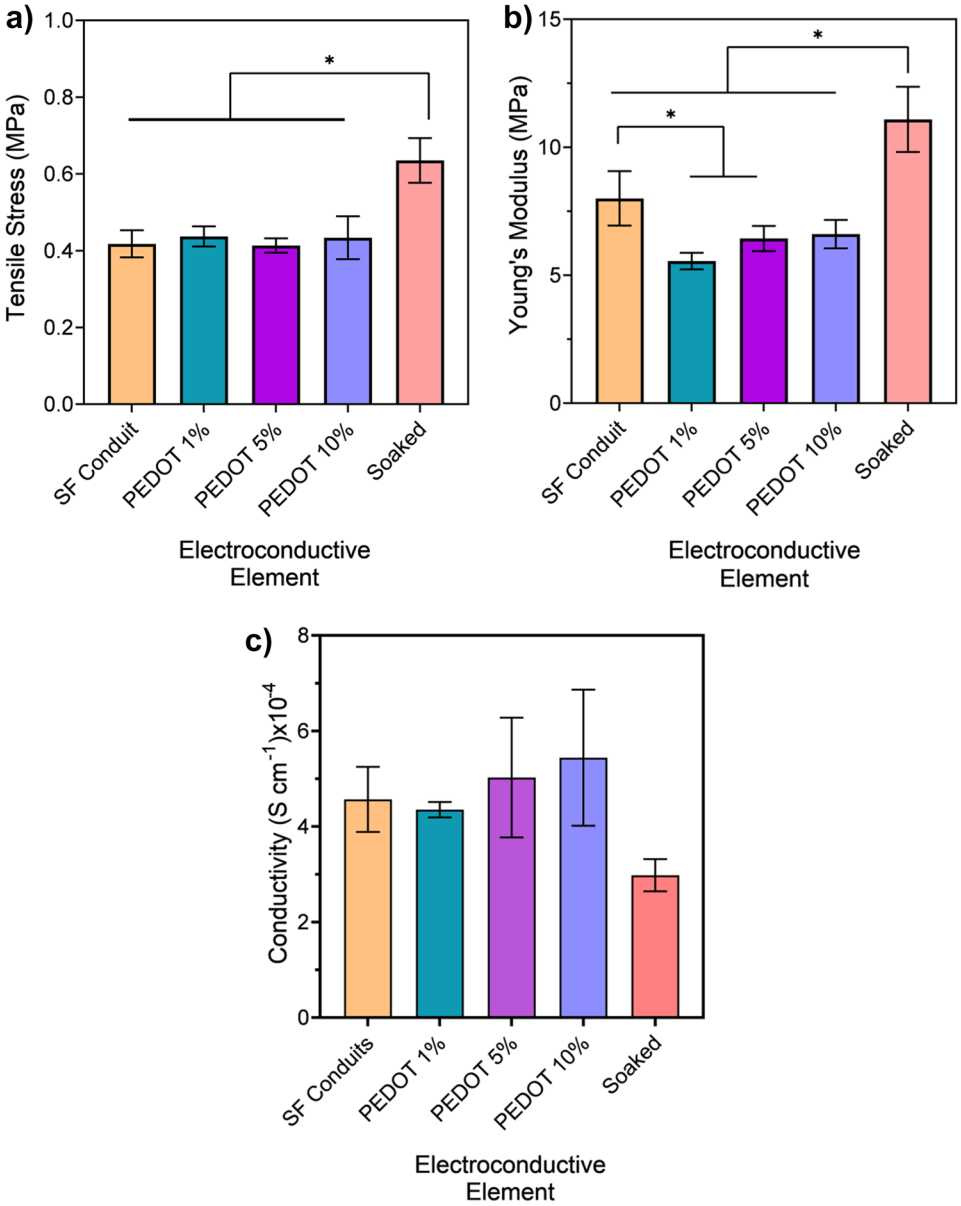

Fig. 8 Mechanical properties of the developed silk-based conduits with **a** Tensile modulus and **b** Young's modulus, $*p < 0.05$, ($n = 5$ samples, mean ± SD). **c** Conductivity of the developed silk-based conduits, $*p < 0.05$, ($n = 3$ samples, mean ± SD)

SF conduits prepared without PEDOT NPs do not exhibit a difference in the tensile stress when they were subjected to 12% strain: 0.42 ± 0.04, 0.44 ± 0.03, 0.42 ± 0.02, and 0.43 ± 0.06 MPa for SF and 1, 5, and 10% of PEDOT NPs-loaded SF conduits, respectively. However, when the PEDOT NPs were incorporated into the conduit via soaking, the tensile stress for 12% strain increases to 0.64 ± 0.06 MPa. These results were consistent with the XPS results. As the NP penetrate the conduits deeper, they act as a composite filler, reinforcing the mechanical properties of the conduits. This effect was particularly increased by the presence of larger pore system that were introduced by the soaking method.

Literature has reported that porcine peroneal and tibial nerves have a Young's modulus of around 7 MPa, a value which was in consonance with the values obtained here [59]. One, five, or ten percent PEDOT NPs conduits were observed to be the stiffest, with a Young's modulus of 5.55 ± 0.32, 6.43 ± 0.49, and 6.61 ± 0.55 MPa, respectively. The Young's modulus for SF conduits was 8 ± 1.06 MPa, which was slightly higher when compared to the conduits with PEDOT NPs. The stiffness of the SF conduits soaked in PEDOT increases significantly, compared to other conduits, recording a modulus of 11.09 ± 1.27 MPa and this may be attributed to restrictions in chain movements within the SF caused by increased levels of NPs, which act as a filler within the silk fibroin matrix.

Conduits may also be placed in flexible body parts, what may subject them to bending and potentially result in occlusion, which was undesired for this application. Kinking resistance was evaluated by bending the conduits

to 50°, as shown in Fig. 9. Interestingly, the FDA-approved NeuraGen conduit collapses at this angle of bending [60]. When conduits were made of SF only, soaked in PEDOT NPs or loaded with low concentrations of PEDOT NPs (1 and 5%), they can be bent at 50° without occlusion (Fig. 9(a)). However, when conduits were loaded with 10% of PEDOT NPs, the collapse point was achieved before bending the conduit to 50°. Moreover, the conduits need to be suitable for suturing to allow their deployment in surgical implants, while maintaining structural integrity and stability during the surgery. To test if these conduits were suitable for grafting, suturability tests were performed by inserting a 4–0 surgical suture (Fig. 9(b), Videos 1, 2, 3 and 4), with all of the conduits sutured successfully.

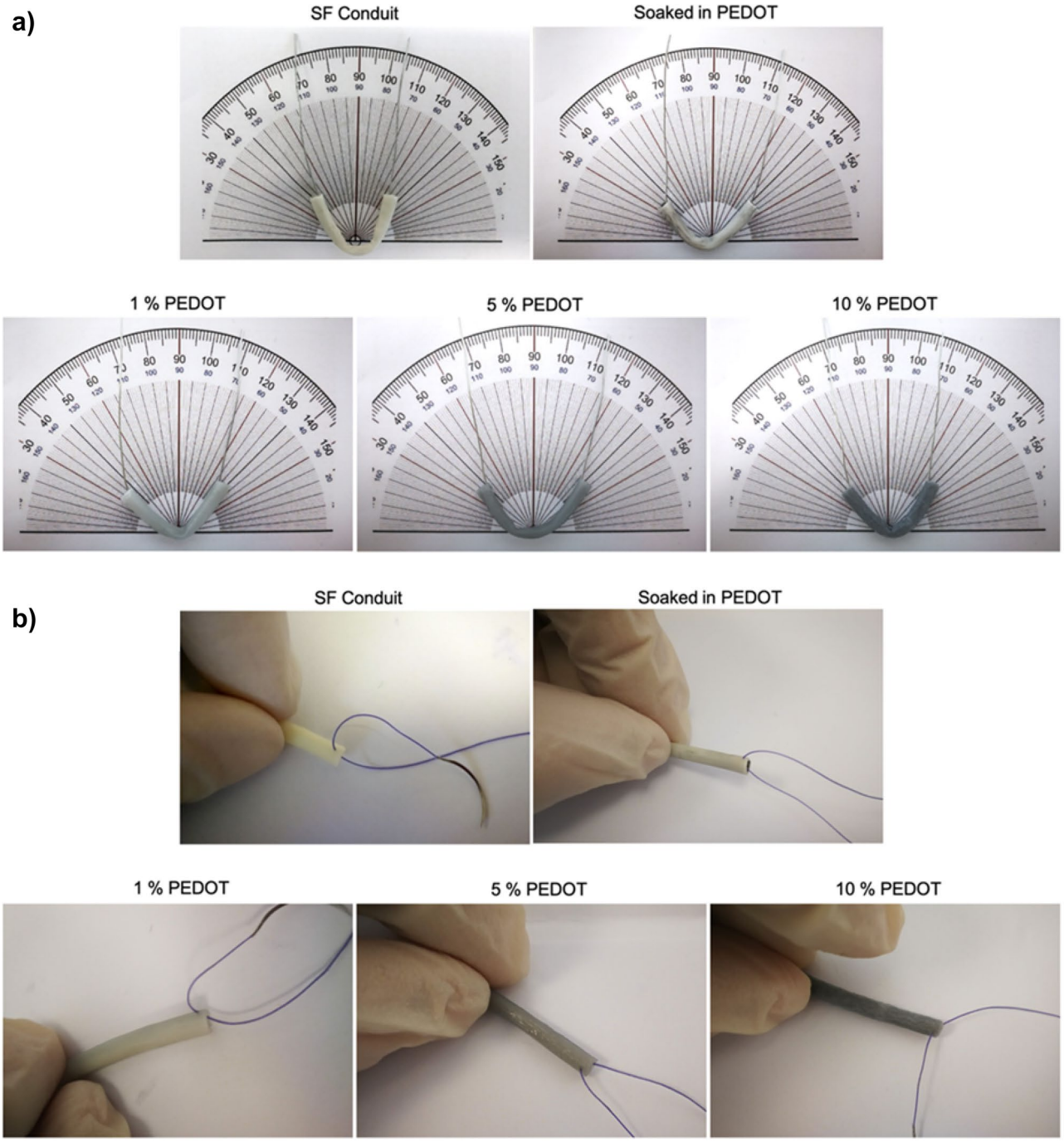

Fig. 9 **a** Kinking and **b** suturability tests performed on control SF conduits, soaked in PEDOT NPs and 1, 5, and 10% PEDOT NPs-loaded SF conduits

3.5 Conductive properties of the conduits

The presence of PEDOT NPs should infer the conduits with conductive properties that enhances the regeneration of nerves and allows for the avoidance of muscle innervation while the nerve regenerates. Figure 8(c) shows the results of the electrical conductivity measurements of the conduits. Wet conduits have been tested, with small differences observed between the samples. The values obtained were in the range of 3–5.4 · 10^{-4} S cm^{-1} which were mainly attributed to the presence of ionic species in the water within the conduits. The small changes observed in the electrical conductivity of the conduits with the addition of PEDOT NPs indicate that the percolation threshold has not been reached due to their particular low aspect ratio and the small concentration of NPs in the conduits. Thus, the electric transport within the conduits was mainly dominated by the ionic contribution to the electrical conductivity whereas the intrinsic electronic contribution provided by the PEDOT NPs only produces a small increase. However, the addition of NPs does increase the conductivity of the samples, particularly when comparing the SF control with no NPs at 4.6 · 10^{-4} ± 0.6 · 10^{-4} S cm^{-1} to that of the 10% PEDOT NP sample at 5.4 · 10^{-4} ± 1.4 · 10^{-4} S cm^{-1}. A similar trend was observed for the dried samples shown in Fig. S3, with a doubling of the electrical conductivity in the presence of PEDOT NPs load of 10% in solution. The SF conduit soaked in the PEDOT NPs has a lower conductivity possibly due to the high dispersibility of the NPs taken up by the system, which in turn reduces the interactions in the system.

3.6 Biocompatibility of the PEDOT NPs

Alamar Blue assay was used to determine the changes in the proliferation rates of MSCs seeded in the presence of PEDOT NPs over a period of 96 h to determine the potential cytotoxic effects. The results of the cellular proliferation measured in 24 h intervals over a period of 96 h were presented in Fig. 10(a). The proliferation of cells cultured in presence of 5 and 10% PEDOT NPs were low if compared to the proliferation of cells cultured in medium. Lowering the concentration of the PEDOT NPs to 1% improves the proliferation of the MSCs with the AB reduction (au) at 31.5 ± 3.5% at 96 h and for the control group at 46.4 ± 5.4%. Two-way ANOVA showed statistically significative differences in the proliferation rates of cells between cells cultured in the presence of medium only compared to the increasing concentrations of PEDOT NPs and the control group.

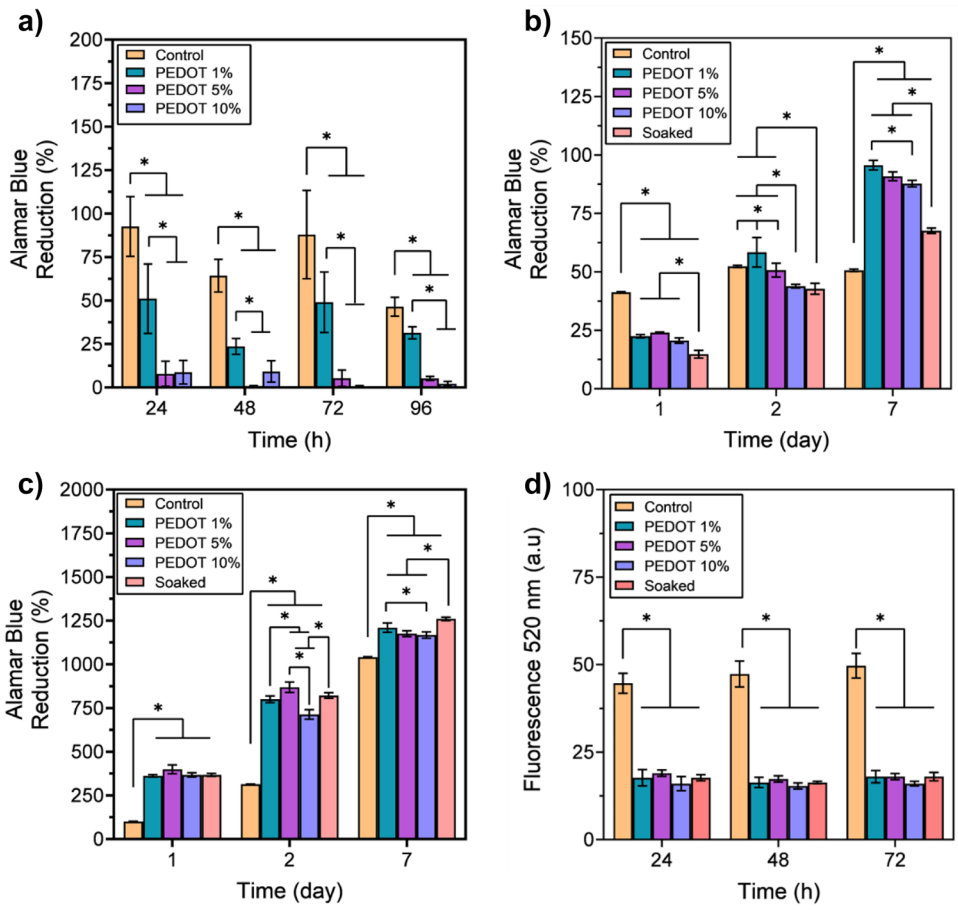

Fig. 10 In vitro testing of PEDOT NP conduits. **a** MSCs viability cultured in presence of PEDOT NPs. As control, MSCs cultured in medium were used. **b** SCs and **c** BJ fibroblasts viability cultured on top of conduits. As control, cells were seeded on adherent culture plates. **d** Fluorescence quantitative measurement of infiltrating BJ fibroblasts. Bottom reading at 485/520 nm excitation/emission set. The control represents cells directly cultured on top of the chamber, $*p < 0.05$, ($n = 3$ samples, mean ± SD)

Though the results may appear to not be favorable in terms of cytotoxic effects, a possible mitigating explanation could arise from the experimental set up. Cell culture plates are often treated to have a negative charge on the well surface to allow for the successful adhesion of cells by means of encouragement of nonspecific surface absorption of serum proteins contained within the media [61]. Due to the difference in the charge between the plates and the PEDOT NPs, the PEDOT NPs could form a film on the surface of the cells due to the electrostatic interaction. This could potentially inhibit the MSCs from oxygen and nutrient diffusion, hence not allowing the cells to proliferate adequately [34]. Therefore, the results presented could not necessarily translate to the effects that the PEDOT NPs-loaded SF conduits would have in vitro.

3.7 Bioactivity of the conduits

Nerve guidance conduits should not calcify when they are implanted considering their application in peripheral nerve repair. To test the developed conduit's apatite-forming ability the conduits were soaked in SBF solution. Table S1 shows the weight percentage of calcium (Ca) and phosphorous (P) ions detected on the surface of conduits through EDS after 1 and 15 days of exposure the SBF. Results after 30 days of exposure were shown in Table 3. The results confirm that all of the tested conduits do not have apatite-forming capacity as the values for Ca and P in every tested conduit is very low and does not represent the formation of apatite [62].

3.8 In vitro biological activity of the conduits

Nerve guidance conduits should provide a supportive luminal surface for proliferation of SCs after a peripheral nerve injury occurs, as these cells play a key role in the regeneration process [63]. For this purpose, SCs were directly seeded in the interior surface of the conduits and their viability was evaluated, with results shown in Fig. 10(b). These results give information about the possible toxicity that the PEDOT NPs could introduce into the system, as they have been seen to influence cell viability. However, the results did not show any toxic effects coming from the PEDOT NPs when they were incorporated into the SF conduits. At 24 h of culture it seems that the presence of PEDOT NPs would affect the

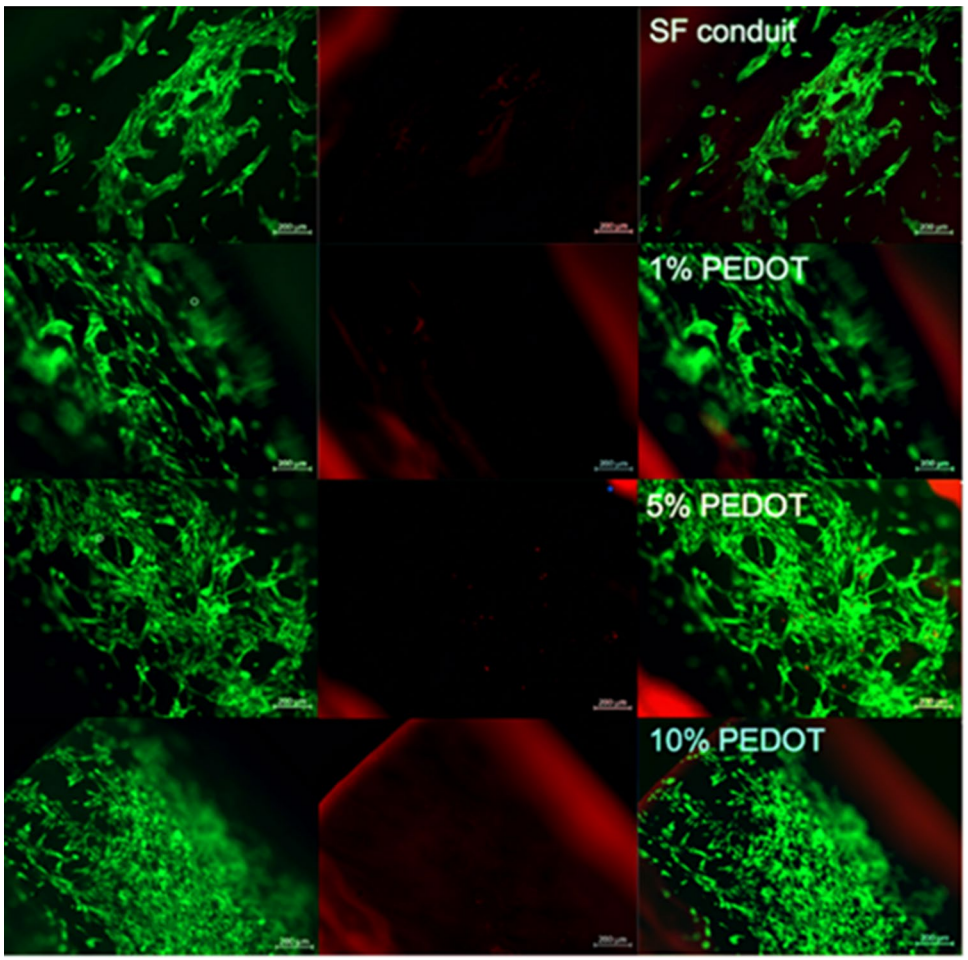

Fig. 11 LIVE/DEAD staining demonstrating the presence of viable/dead SCs after 72 h of culturing on the interior surface of the conduits. First column are images of green channel, which represent the live cells, capable of migration. The second column are red channel images, representing dead cells. Third column shows the merged images of green and red channels

proliferation of SCs, but at 72 h the effect was reversed for 1 and 5% PEDOT NPs-loaded SF conduits. SCs cultured on top of 10% PEDOT NPs-loaded SF conduits and SF conduits soaked in PEDOT NPs decrease the proliferation rate when compared to the SF conduit control group with no NPs. After 7 days of culture, the proliferation was enhanced for every cell group cultured on top of PEDOT NPs-loaded SF conduits and the viability was significantly higher when compared to the control group. Increasing the concentration of the NP decreases the viability of the SC cells to a small degree, though it should be noted that the SF conduit with no PEDOT NPs had a significantly lower viability rate. It could be hypothesized that the concentration of the NPs must be controlled to obtain a desired cellular output suggesting a duality in the cellular response to the PEDOT NPs.

The same in vitro experiment was performed with BJ fibroblasts to study their proliferation on PEDOT NPs-loaded SF conduits. Figure 10(c) shows the results at 24 h, 72 h, and 7 days of culture. In this case, BJ fibroblasts have shown an improved proliferation since the first day of culture. It has been demonstrated that the PEDOT NPs-loaded SF conduits do not have a negative effect on SCs and BJ fibroblasts proliferation. It could be hypothesized that the addition of a conductive platform allows for a greater proliferation of cells, perhaps due to a controlled cellular microenvironment within the conductive conduits [15–17].

LIVE/DEAD staining allowed to qualitatively confirm the previous results of SCs culturing in Fig. 11. Figure S4 shows fluorescence microscopy images of SCs cultured on top of SF conduits and 1, 5, and 10% NPs-loaded SF conduits for 24 h. There was little presence of dead cells (red cannel) that can be observed for all the tested conduits; however, it can be clearly seen that cells proliferate through the conduits without any alarming cell death (green channel).

Figure 10(d) shows the result of infiltrating cells through the conduit. It was highly important to avoid cells that can promote scar formation entering the lumen of the conduit. If fibroblasts enter and form scar tissue, nerve regeneration would be impaired [40]. As can be seen in the graph, BJ fibroblasts cannot infiltrate through either of the conduits as the pore size of the conduits is lower than the cellular size of the fibroblasts [42]. The control refers to BJ fibroblasts seeded directly on top of the membrane of the Boyden Chamber. These results were confirmed qualitatively by fluorescence imaging in Fig. S5, with images of the bottom of the well taken to observe BJ fibroblasts that passed through the membrane. These results indicate that fibroblasts should not be able to enter the lumen of the developed conduits and induce scar formation inside the graft, thus preventing the termination of the nerve regeneration process.

4 Conclusions

In this study, novel PEDOT NPs were combined with silk fibroin to create conduits for targeted PNI repair. The specified manufacturing process allows for the synthesis of novel morphologically round and stable PEDOT NPs with a diameter of 187 ± 20.2 nm. The developed conduits have good properties in terms of porosity and physico-chemical properties. The synthesized conduits were prepared with three different concentrations of PEDOT NPs. In every case the mechanical properties of the conduits match closely to the tensile modulus of native tissue, ranging from 5.55 ± 0.32 to 6.61 ± 0.55 MPa. The conduits also exhibit good flexibility with a kinking resistance up to angles of 50° achieved for nearly all conduit specifications without occlusion of the conduits observed. The conduits were also not disrupted when subjected to suturing. The PEDOT NPs-loaded SF were also electroactive, due to the presence of the conductive PEDOT NPs. Bioactivity studies with SBF show that the PEDOT NPs-loaded SF conduits do not possess apatite-forming capacity. Regarding the bioactivity of the conduits, although PEDOT NPs show some cytotoxic effect, the conduits do not display the same characteristics. The conduits demonstrated to be a good surface for SCs proliferation, and moreover, they did not allow BJ fibroblasts infiltration, avoiding scar tissue formation in the lumen. The SF conduits combined with novel PEDOT NPs outlined above show great promise for the purpose of PNI repair.

Supplementary Information The online version contains supplementary material available at https://doi.org/10.1007/s42114-023-00689-2.

Author contribution A.E., A.S., A.B., M.R.C., and M.C.: data curation. A.E., A.S., A.B., M.R.C., M.C., J.M.O., R.L.R., and M.N.C.: writing of the manuscript. J.M.O., A.C., R.L.R., and M.N.C.: supervision. A.E, A.S., A.B., J.M.O., A.C., R.L.R., and M.N.C.: revision of the manuscript. A.S., M.N.C., and J.M.O.: funding acquisition.

Funding Open access funding provided by FCT|FCCN (b-on). This study received financial support from the Portuguese Foundation for Science and Technology under the distinction attributed to JMO (IF/01285/2015) and the project NanOptoNerv (ref. PTDC/NAN-MAT/29936/2017), the European Commission and FEDER program under the JUSTHera project (NORTE-01-0145-FEDER-000055) and the 0624_2IQBIONEURO_6_E project (Inter-regional cooperation program VA Spain-Portugal POCTEP 2014–2020), and the Irish Research Council under EPSPG/2020/78 and New Foundations Grant 2019.

Data availability The raw/processed data required to reproduce these findings cannot be shared at this time as the data also forms part of an ongoing study.

Declarations

Conflict of interest The authors declare no competing interests.

References

1. Taylor CA et al (2008) The incidence of peripheral nerve injury in extremity trauma. Am J Phys Med Rehabil 87(5):381–385
2. Hussain G et al (2020) Current status of therapeutic approaches against peripheral nerve injuries: a detailed story from injury to recovery. Int J Biol Sci 16(1):116–134
3. Bhandari PS (2019) Management of peripheral nerve injury. J Clin Orthop Trauma 10(5):862–866
4. Yi S et al (2020) Application of stem cells in peripheral nerve regeneration. Burn Trauma 8:tkaa002
5. Kuang T et al (2022) A facile approach to fabricate load-bearing porous polymer scaffolds for bone tissue engineering. Adv Compos Mater 5(2):1376–1384
6. Basak S (2021) Redesigning the modern applied medical sciences and engineering with shape memory polymers. Adv Compos Mater 4(2):223–234
7. Arslantunali Şahin D et al (2014) Peripheral nerve conduits: technology update. Med Devices Evid Res 7:405–424
8. Moore AM et al (2009) Limitations of conduits in peripheral nerve repairs. Hand (New York, N.Y.) 4(2):180–186
9. Sun W et al (2021) Silk fibroin as a functional biomaterial for tissue engineering. Int J Mol Sci 22(3)
10. Melke J et al (2016) Silk fibroin as biomaterial for bone tissue engineering. Acta Biomater 31:1–16
11. Boni BOO et al (2020) Combining silk sericin and surface micropatterns in bacterial cellulose dressings to control fibrosis and enhance wound healing. Eng Sci 10:68–77
12. Bakadia BM et al (2022) Biodegradable and injectable poly(vinyl alcohol) microspheres in silk sericin-based hydrogel for the controlled release of antimicrobials: application to deep full-thickness burn wound healing. Adv Compos Mater 5(4):2847–2872
13. Boni BOO et al (2022) In vivo performance of microstructured bacterial cellulose-silk sericin wound dressing: effects on fibrosis and scar formation. Eng Sci 19:175–185
14. Vyas S et al (2022) High performance conducting nanocomposites polyaniline (PANI)-CuO with enhanced antimicrobial activity for biomedical applications. ES Mater Manuf 15:46–52
15. Hu M et al (2019) Electrical stimulation enhances neuronal cell activity mediated by Schwann cell derived exosomes. Sci Rep 9(1):1–12
16. Banks TA et al (2015) Effects of electric fields on human mesenchymal stem cell behaviour and morphology using a novel multichannel device. Integr Biol (United Kingdom) 7(6):693–712
17. McCaig CD, Zhao M (1997) Physiological electrical fields modify cell behaviour. BioEssays 19(9):819–826
18. Fang X et al (2020) Conductive conduit small gap tubulization for peripheral nerve repair. RSC Adv 10(28):16769–16775
19. Nezakati T et al (2019) Ultra-low percolation threshold POSS-PCL/graphene electrically conductive polymer: Neural tissue engineering nanocomposites for neurosurgery. Mater Sci Eng C Mater Biol Appl 104:109915
20. Huang Z et al (2020) Tracing carbon nanotubes (CNTs) in rat peripheral nerve regenerated with conductive conduits composed of poly(lactide-co-glycolide) and fluorescent CNTs. ACS Biomater Sci Eng 6(11):6344–6355
21. Kuzmenko V et al (2018) Tailor-made conductive inks from cellulose nanofibrils for 3D printing of neural guidelines. Carbohyd Polym 189:22–30
22. Steel EM, Azar J-Y, Sundararaghavan HG (2020) Electrospun hyaluronic acid-carbon nanotube nanofibers for neural engineering. Materialia 9:100581
23. Farzamfar S et al (2019) A novel polycaprolactone/carbon nanofiber composite as a conductive neural guidance channel: an in vitro and in vivo study. Prog Biomater 8(4):239–248
24. Kobayashi N, Izumi H, Morimoto Y (2017) Review of toxicity studies of carbon nanotubes. J Occup Health 59(5):394–407
25. Saleemi MA et al (2021) Toxicity of carbon nanotubes: molecular mechanisms, signaling cascades, and remedies in biomedical applications. Chem Res Toxicol 34(1):24–46
26. Alizadeh R et al (2019) Conductive hydrogels based on agarose/alginate/chitosan for neural disorder therapy. Carbohydr Polym 224
27. Vijayavenkataraman S et al (2019) 3D-printed PCL/PPy conductive scaffolds as three-dimensional porous nerve guide conduits (NGCs) for peripheral nerve injury repair. Front Bioeng Biotechnol 7:266
28. Bagher Z et al (2019) Conductive hydrogel based on chitosan-aniline pentamer/gelatin/agarose significantly promoted motor neuron-like cells differentiation of human olfactory ecto-mesenchymal stem cells. Mater Sci Eng C Mater Biol Appl 101:243–253
29. Zhao Y et al (2020) Application of conductive PPy/SF composite scaffold and electrical stimulation for neural tissue engineering. Biomaterials 255:120164
30. Kim S et al (2018) Versatile biomimetic conductive polypyrrole films doped with hyaluronic acid of different molecular weights. Acta Biomater 80:258–268
31. Wang Y et al (2017) A highly stretchable, transparent, and conductive polymer. Sci Adv 3(3):e1602076
32. Yang Y, Deng H, Fu Q (2020) Recent progress on PEDOT:PSS based polymer blends and composites for flexible electronics and thermoelectric devices. Mater Chem Front 4(11):3130–3152
33. Mantione D et al (2017) Poly(3,4-ethylenedioxythiophene) (PEDOT) derivatives: innovative conductive polymers for bioelectronics. Polymers 9(8):354
34. Serafin A, Culebras M, Oliveira JM, Koffler J, Collins MN (2023) 3D printable electroconductive gelatin-hyaluronic acid materials containing polypyrrole nanoparticles for electroactive tissue engineering. Adv Compos Hybrid Mater 6(3):109
35. Yan LP et al (2016) Tumor growth suppression induced by biomimetic silk fibroin hydrogels. Sci Rep 6:31037
36. Kokubo T, Takadama H (2006) How useful is SBF in predicting in vivo bone bioactivity? Biomaterials 27(15):2907–2915
37. Bružauskaitė I et al (2016) Scaffolds and cells for tissue regeneration: different scaffold pore sizes-different cell effects. Cytotechnology 68(3):355–369
38. Murphy CM, O'Brien FJ (2010) Understanding the effect of mean pore size on cell activity in collagen-glycosaminoglycan scaffolds. Cell Adh Migr 4(3):377–381
39. Tao J et al (2017) A 3D-engineered porous conduit for peripheral nerve repair. Sci Rep 7(1):46038
40. Ezra M et al (2016) Porous and nonporous nerve conduits: the effects of a hydrogel luminal filler with and without a neurite-promoting moiety. Tissue Eng Part A 22(9–10):818–826

41. Kokai LE et al (2009) Diffusion of soluble factors through degradable polymer nerve guides: controlling manufacturing parameters. Acta Biomater 5(7):2540–2550
42. Uhal BD et al (1998) Cell size, cell cycle, and α-smooth muscle actin expression by primary human lung fibroblasts. Am J Physiol Lung Cell Mol Physiol 275(5):L998–L1005
43. Lu Q et al (2010) Water-insoluble silk films with silk I structure. Acta Biomater 6(4):1380–1387
44. Meinel L, Kaplan DL (2012) Silk constructs for delivery of musculoskeletal therapeutics. Adv Drug Deliv Rev 64(12):1111–1122
45. Freddi G, Tsukada M, Beretta S (1999) Structure and physical properties of silk fibroin/polyacrylamide blend films. J Appl Polym Sci 71(10):1563–1571
46. Zhao Q et al (2014) The structure and properties of PEDOT synthesized by template-free solution method. Nanoscale Res Lett 9(1):557
47. Deetuam C et al (2014) Synthesis of well dispersed graphene in conjugated poly(3,4-ethylenedioxythiophene): polystyrene sulfonate via click chemistry. Compos Sci Technol 93:1–8
48. Cheng Y-H et al (2014) Poly(3,4-ethylenedioxythiophene) (PEDOT) hollow microflowers and their application for nitrite sensing. Sens Actuator B Chem 192:762–768
49. Xiao Y et al (2012) Electrodeposition of high performance PEDOT/Ti counter electrodes on Ti meshes for large-area flexible dye-sensitized solar cells. Electrochim Acta 85:432–437
50. Magoshi J, Nakamura S (1975) Studies on physical properties and structure of silk. Glass transition and crystallization of silk fibroin. J Appl Polym Sci 19(4):1013–1015
51. Johari N, Moroni L, Samadikuchaksaraei A (2020) Tuning the conformation and mechanical properties of silk fibroin hydrogels. Eur Polymer J 134:109842
52. Khan MA et al (2000) Surface characterization of poly(3,4-ethylenedioxythiophene)-coated latexes by X-ray photoelectron spectroscopy. Langmuir 16(9):4171–4179
53. Niu Y et al (2021) Effect of poly(diallyldimethylammonium chloride) adsorption on the dispersion features of SiC particles in aqueous media. New J Chem 45(10):4638–4646
54. Heidemann SR, Buxbaum RE (1994) Mechanical tension as a regulator of axonal development. Neurotoxicology 15(1):95–107
55. Bueno FR, Shah SB (2008) Implications of tensile loading for the tissue engineering of nerves. Tissue Eng Part B Rev 14(3):219–233
56. Nectow AR, Marra KG, Kaplan DL (2012) Biomaterials for the development of peripheral nerve guidance conduits. Tissue Eng Part B Rev 18(1):40–50
57. Luis AL et al (2007) Evaluation of two biodegradable nerve guides for the reconstruction of the rat sciatic nerve. Bio-Med Mater Eng 17:39–52
58. Rydevik BL et al (1990) An in vitro mechanical and histological study of acute stretching on rabbit tibial nerve. J Orthop Res 8(5):694–701
59. Zilic L, Wilshaw SP, Haycock JW (2016) Decellularisation and histological characterisation of porcine peripheral nerves. Biotechnol Bioeng 113(9):2041–2053
60. Clements BA et al (2016) Design of barrier coatings on kink-resistant peripheral nerve conduits. J Tissue Eng 7:2041731416629471
61. Lerman MJ et al (2018) The evolution of polystyrene as a cell culture material. Tissue Eng Part B Rev 24(5):359–372
62. Pasero M et al (2010) Nomenclature of the apatite supergroup minerals. Eur J Mineral 22(2):163–179
63. Yang Y et al (2007) Biocompatibility evaluation of silk fibroin with peripheral nerve tissues and cells in vitro. Biomaterials 28(9):1643–1652